

# TRANSIENT SIMULATION OF A SUPERCRITICAL CARBON DIOXIDE (sCO<sub>2</sub>) CONCENTRATED SOLAR POWER (CSP) SYSTEM

R. van der Westhuizen<sup>1</sup> and R.T. Dobson<sup>2</sup>

Department of Mechanical and Mechatronic Engineering, Stellenbosch University, Stellenbosch, South Africa

<sup>1</sup> rvanderwesthuizen@sun.ac.za

<sup>2</sup> rtd@sun.ac.za

## Abstract

There will always be a need for off-grid electrical power production; whether to support rural communities or to drive industrial activities such as mining or agriculture. Off-grid electrical power is often sourced from polluting sources, such as diesel generators. However, South Africa has abundant sunshine and is well-positioned to take advantage of concentrated solar power (CSP) – a proven renewable and non-polluting energy source. Whilst the ubiquitous steam Rankine cycle is suitable for CSP, it is only appropriate for large-scale electrical power production. The supercritical carbon dioxide (sCO<sub>2</sub>) Brayton cycle is a promising alternative to the steam Rankine cycle; and provides many new opportunities for CSP, especially for space-sensitive applications. This work explores sCO<sub>2</sub> as a working fluid and proposes the system layout for a potential small-scale CSP plant. The methodology used to model and simulate this system is then presented. The success of the simulation relies on accurate modelling, and the models of some of the most important elements in the system are therefore showcased. The purpose of the simulation is to attain an insight into the relationships between the elements of the system at design- as well as off-design conditions – such as during start-up, shut-down and changing environmental conditions.

*Keywords: Concentrated Solar Power (CSP); Supercritical Carbon Dioxide (sCO<sub>2</sub>); Brayton Cycle; Solar Thermal Energy; Renewable Energy*

## 1. Introduction

Most large-scale electrical power is generated using some kind of heat source and a thermodynamic cycle [1], and the steam Rankine cycle is the de facto choice for the majority of heat sources and applications [2]. Whilst water has many advantages as a working fluid, there are also some drawbacks [3]. One of the main benefits that a sCO<sub>2</sub> cycle has over a steam cycle is far smaller equipment for a similar thermodynamic efficiency [4]. This presents an opportunity for CSP to be used in applications where it is not feasible if steam is used, such as in micro- and small-scale off-grid electrical power production.

## 2. sCO<sub>2</sub> as Working Fluid

As a result of the high supercritical density of CO<sub>2</sub>, for the same mass flow rate and work output, a sCO<sub>2</sub> turbine will be much smaller than a steam turbine [5]. But there are additional benefits of sCO<sub>2</sub> as well: the higher density reduces the compressor work, which in turn increases the thermodynamic cycle efficiency [6]; the relatively low critical temperature makes sCO<sub>2</sub> cycles amenable to dry cooling [7] (which is advantageous in water-scarce areas) and sCO<sub>2</sub> has many of the same characteristics as steam – it is abundant, inexpensive, non-flammable and non-toxic. Furthermore, sCO<sub>2</sub> cycles are well-suited to be adapted to process heat co-generation if desired, which further extends its capability and reduces (or removes outright) the need for a cycle heat sink.

One of the challenges with sCO<sub>2</sub> as working fluid is that the significant changes of the specific heat capacity around the critical point makes heat exchanger design particularly difficult [2]. Also, CO<sub>2</sub> can be corrosive under certain conditions which makes material selection an important consideration [7].

### 3. Justification of the Project

#### 3.1. Comparisons to Previous Simulations

Simulations that have been completed previously by others have served to fulfill different purposes. Whilst each simulation has surely made significant contributions to the understanding of sCO<sub>2</sub> and/or CSP-sCO<sub>2</sub> systems, it appears that no other simulation fulfills quite the same purpose as this work. For example, the simulations by [8,9,10] are detailed, but do not investigate the solar aspects (e.g. the solar receiver). On the other hand, [7,11] discuss the solar aspects, but only study the design point. [12,13] performed transient investigations of several CSP-sCO<sub>2</sub> system layouts but applied rather simplistic component models.

This project aims to merge the superior aspects of the previous simulation efforts and create a detailed, transient model of a sCO<sub>2</sub> cycle, while giving adequate consideration to the CSP aspects. Also, unlike the other simulations (which were typically performed using professionally developed, specialised computer codes such as TRNSYS, SAM, GT-SUITE, MARS, SteamPro or PEACE), this project is coded from first principles. This has two distinct advantages: the variables characterising each component have a direct and visible impact on the performance of the entire system; and it allows for more precise control over the modelling.

For example, a variable like the turbine rotor outlet blade angle can be adjusted and its effect on the performance of the cycle can be studied in the same environment as all the other variables, like the solar receiver tube diameter or heat sink fin spacing. This is in contrast to many other simulations where the turbomachinery might be modelled in one environment and the heat exchangers in another.

The software selected to develop the models and simulation for this project is MATLAB by MathWorks, for the following reasons:

- Large collection of built-in functions and features that save a great deal of coding time
- Easy to learn, “generic” programming language that can appeal to engineers with different programming backgrounds
- Ability to interface with other programming languages, including C and Fortran
- Cross-platform compatibility, including Microsoft Windows, Apple macOS and Linux
- Excellent help and support documentation, guides, examples and online forums

#### 3.2. Applicability of the Results

At its completion, this simulation should be a useful tool not only in designing and optimising CSP-sCO<sub>2</sub> systems, but also in developing control strategies for such systems.

Theoretical modelling and experimental validation are both needed for the success of any CSP-sCO<sub>2</sub> system. Unfortunately, there have been few physical sCO<sub>2</sub> cycle experiments to date, none of which have been integrated with CSP. By linking component design variables and system performance parameters at design- and off-design conditions, this simulation would allow potential designs to be studied in detail and optimised, such that future experiments could be conducted in a focused and meaningful way.

Although the simulation is performed for a small-scale CSP plant, the results of the simulation are definitely not limited to this realm only. The results may provide insight into general sCO<sub>2</sub> cycles – including small- and large-scale cycles and cycles powered by other heat sources, including nuclear, biomass or fossil-fuel plants.

#### 3.3. Validation

The shortage of relevant experimental data poses a challenge to validating the modelling and simulation results of this project. After all, it is this shortage that the project in some way hopes to address. Having said that, the modelling and simulation results can still be validated against the results of other numerical studies.

Currently, as one of the most intensive sCO<sub>2</sub> projects, the state-of-the-art in sCO<sub>2</sub> Brayton cycle modelling is arguably the Sandia National Laboratories project, explained and analysed by [10]. The turbomachinery models presented by [10] can be used to validate the turbomachinery models of this project, whereas the heat exchanger models can be validated and compared with the results of [14,15].

### 4. The CSP-sCO<sub>2</sub> System

#### 4.1. Overview

Although many different Brayton cycle configurations exist [16], all of them utilise the same three basic elements: compressors, turbines and heat exchangers. The configuration chosen for this simulation is the simple *recuperated Brayton cycle*. It consists of a single compressor, a single turbine and three heat exchangers: one which receives heat from a heat source (in this case the heat source is concentrated sunlight), another which removes heat from the cycle to the environment and a third *recuperator* heat exchanger which uses waste heat from the stream exiting the turbine to pre-heat the stream going towards the solar receiver.

The recuperator improves the thermodynamic efficiency of the cycle by reducing the required heat input at the solar receiver.

A schematic diagram of the system layout is presented in Fig. 1 and a T-s diagram of the fluid cycle is presented in Fig. 2. The temperatures and pressures shown in Fig. 2 are approximate, because the simulation will be transient, and the instantaneous operating conditions may differ substantially from the steady-state design values. The CO<sub>2</sub> vapour dome and critical point are indicated in Fig. 2 for reference.

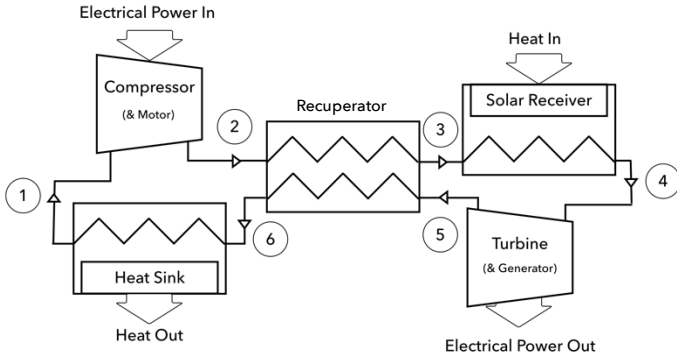


**Fig. 1. Schematic diagram of the system layout (adapted from [16])**

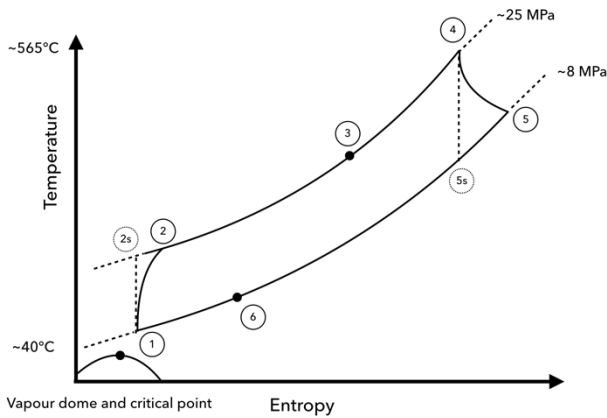


**Fig. 2. T-s diagram of the fluid cycle (adapted from [16])**

A fourth heat exchanger (not shown) may be installed between the end of the solar receiver and the inlet to the turbine. This heat exchanger can transfer heat to the thermal energy storage system when there is sufficient solar energy available (e.g. midday, no cloud cover) and re-transfer this stored thermal energy back to the main cycle when it is needed (e.g. during cloudy conditions or night-time). The thermal energy storage system is not modelled in detail for this project.

Whilst the compressor, motor, turbine and generator could be mounted on a single shaft, in this simulation the compressor and motor are mounted on one shaft and the turbine and generator are mounted on a different shaft. This allows for independent modelling and control of each machine.

Design net electrical power output is set at 10MW, which is sufficient for a small-scale grid-independent power plant and is also the ideal capacity that is recommended for future sCO<sub>2</sub> pilot plants [17].

#### 4.2. General Assumptions

As with any general engineering problem, it is necessary to make certain assumptions and simplifications at the outset of the solution process. These assumptions must be made based on the kind of solution required and the level of accuracy sought, whilst remaining within the bounds of engineering theory and computational limits.

The purpose of the simulation is to gain a general understanding of the system's dynamics. The intention is to discover overall trends, not specific numerical values. To this end, the following general assumptions are made (which have been used successfully before by others [8,13]):

- One-dimensional fluid flow
- Quasi-static equilibrium

The fluid is assumed to flow only in the axial- or z-direction, with a constant average velocity across its cross-sectional area. There are no flow components in the other directions at any time (note however that the turbomachinery is analysed using a multi-dimensional method – see §5.2).

In the context of this project, *quasi-static equilibrium* means that the mass flow rate is allowed to vary with time, but not position, i.e.

$$\frac{\partial \dot{m}}{\partial z} \Big|_t = 0$$

or that the spatial derivative of the mass flow rate at a particular time step  $t$  is zero. Equivalently, because the fluid flow is one-dimensional,

$$\dot{m}_{in} \Big|_t = \dot{m}_{out} \Big|_t$$

which states that at a particular time step, the mass flow rate into any control volume in the cycle is equal to the mass flow rate out of the control volume. This may to some extent seem trivial, but it is important to assert this condition. It implies that there is no accumulation of mass anywhere in the system within a particular time interval, which in practice prohibits the solving of sound/shock-waves propagating through the system. Transient effects of the order of nano- and micro-seconds would therefore not be captured by this simulation, but it is also not the purpose of this work. Transient effects of the order of seconds to minutes are more relevant and these are unaffected by the quasi-static equilibrium assumption.

## 5. Modelling

### 5.1. Fundamentals

Any general fluid mechanics problem (provided that sufficient information about the boundary and initial conditions are available) can be solved through the use of four fundamental principles [18]:

- The conservation of mass
- The conservation of momentum
- The conservation of energy
- Equations of state

These four principles are extensively applied in this work. The three *conservation equations* are typically derived on a case-by-case basis. In this work, two different cases are employed: a set of equations used for elemental control volumes (the derivations of which are described in detail by [19]), and a set of equations used for turbomachines (the derivations of which are described in detail by [20]).

The *equation of state* principle asserts that if any two properties of the fluid are known, then all the other fluid properties can be expressed as functions of the two known properties. For example, if temperature  $T$  and pressure  $P$  are known, then the density  $\rho$  of the fluid can be calculated as  $\rho = \rho(T, P)$ . The function  $\rho(T, P)$  is used to calculate an unknown  $\rho$  from known values of  $T$  and  $P$ .

In practice, the equations of state of fluids are not simple functions. Under exceptional circumstances, fluids may be modelled using *perfect gas* or *incompressible* assumptions, in which case the equations of state are indeed simple functions. But in general, and certainly for the case of sCO<sub>2</sub> in the range of operation for this system, the perfect gas and incompressible assumptions are inaccurate, and the equations of state are not straightforward to determine.

There are at least two different ways in which the function  $\rho(T, P)$  can be determined from a table of known  $\rho$ ,  $T$  and  $P$  values. The first is to perform a multi-variable regression analysis; for example

$$\rho \approx c_0 + c_1T + c_2P + c_3TP + c_4T^2 + c_5P^2 \dots$$

where the constants  $c_0$  to  $c_n$  are to be determined. This is easily performed in mainstream spreadsheet packages. The more terms that are included in the analysis, the more accurate the prediction of  $\rho$  becomes.

The other method is to derive an interpolating function between known data points. More data points allow for more accurate interpolation. A numerical computing package such as MATLAB has this functionality built-in.

The same methods can be applied to other combinations of the thermodynamic data of CO<sub>2</sub>, and expressions for any variable as a function of any two others can be determined in this way.

### 5.2. Turbomachinery

Turbomachinery in the context of this work refers to the turbine and compressor. Details of the turbine model are discussed below – the compressor is modelled in a similar fashion.

The purpose of a turbine is to transfer energy from a continuous fluid stream to a set of blades mounted on a rotating shaft [20]. Consider a schematic diagram of a turbine in Fig. 3.

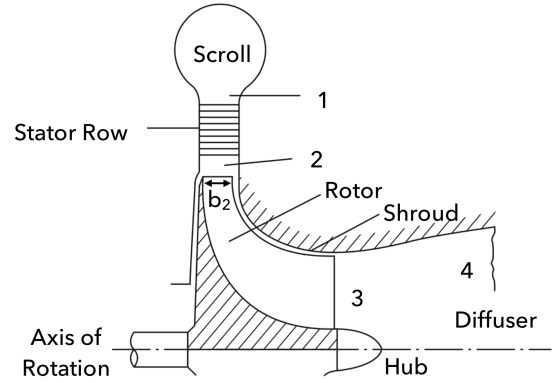


**Fig. 3. Schematic diagram of a turbine; view along the axis of rotation (adapted from [20])**

After passing through upstream components in the cycle, fluid enters the scroll (station 1) at a relatively high pressure and a relatively low velocity. The scroll passage becomes smaller, reducing the pressure and increasing the velocity of the flow. The fluid passes through the stator row where nozzles turn the flow such that it arrives at the inlet of the rotor blades (station 2) in the radial and tangential directions. The fluid leaves the rotor blades (station 3) predominantly in the axial direction.

Finally, the diffuser section slows the fluid through an expanding channel, recovering pressure in the process. Flow leaves the diffuser (station 4) and continues to the downstream components of the cycle.

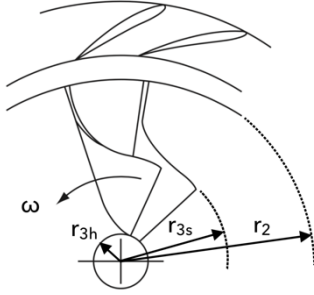
If the blade thickness is assumed to be negligible, the radial flow area at the rotor inlet  $A_{2r}$  is the disc defined by blade radius  $r_2$  and width  $b_2$ :

$$A_{2r} = 2\pi r_2 b_2$$

The axial flow area at the rotor outlet  $A_{3x}$  is the annulus defined by blade radius at the hub  $r_{3h}$  and the blade radius at the shroud  $r_{3s}$ :

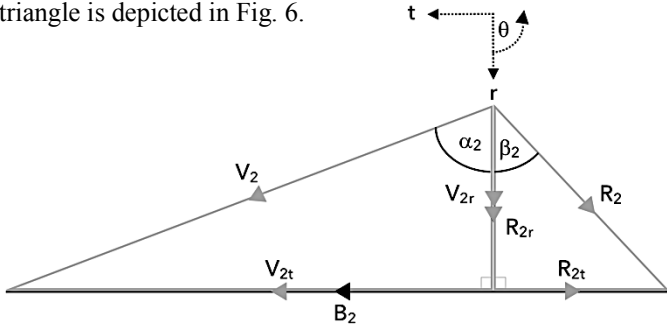
$$A_{3x} = \pi(r_{3s}^2 - r_{3h}^2)$$

Fig. 4 is a schematic diagram of the turbine as viewed perpendicular to the axis of direction and depicts the three radii of interest. The direction of rotation is taken as positive in the counter-clockwise direction (as indicated) and is of a magnitude denoted by  $\omega$ .



**Fig. 4. Schematic diagram of a turbine; view perpendicular to the axis of rotation (adapted from [20])**

It is common practice to model fluid flow through turbomachinery on *axi-symmetric stream surfaces* [20]. This implies that, at the inlet, flow is *only* in the radial and tangential directions; and, at the outlet, flow is *only* in the axial and tangential directions. With these simplifications in mind, one can define two-dimensional *velocity triangles* at the inlet and the outlet of the turbine rotor to relate the absolute velocity vector of the flow  $\mathbf{V}$  to the velocity vector of the rotor blades  $\mathbf{B}$ . The inlet velocity triangle diagram shows the velocity components in the radial ( $r$ ) and tangential ( $t$ ) directions, and the outlet velocity triangle diagram shows the velocity components in the axial ( $x$ ) and tangential directions. The inlet velocity triangle is depicted in Fig. 5, and the outlet velocity triangle is depicted in Fig. 6.



**Fig. 5. Velocity triangle at the inlet of the turbine rotor**

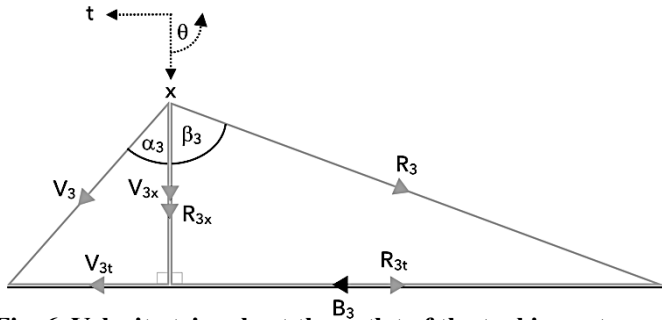


**Fig. 6. Velocity triangle at the outlet of the turbine rotor**

The relative flow velocity vector  $\mathbf{R}$  is obtained by subtracting the blade velocity from the absolute flow velocity:

$$\mathbf{R} = \mathbf{V} - \mathbf{B}$$

At a given radius  $r$  the blade velocity can be expressed as

$$B = \omega r$$

The angle  $\alpha_2$  is a fixed value and corresponds to the angle of the nozzle row at the inlet. Similarly, the angle  $\beta_3$  is a fixed value and corresponds to the blade angle of the rotor at the outlet. In general, angles  $\beta_2$  and  $\alpha_3$  vary depending on the velocities of the fluid and the blade. However, at the *nominal design-point*, it is customary to set  $\beta_2 = \alpha_3 = 0^\circ$  which means that relative flow at the inlet is purely radial, and absolute flow at the outlet is purely axial.

General assumptions that are made include that the turbine is adiabatic, that work is only done in the rotor section (not in the scroll or diffuser sections) and that elevation changes are negligible (which allows gravitational potential energy terms to be ignored).

It is shown by [20] how the fundamental equations can be applied to turbomachinery; only the results are reported here.

Application of the conservation of mass principle yields the following result:

$$\dot{m} = \rho_2 V_{2r} A_{2r} = \rho_3 V_{3x} A_{3x}$$

where  $\dot{m}$  is the mass flow rate through the turbine. Application of the conservation of momentum principle yields:

$$\dot{W} = M\omega = \dot{m}(B_2 V_{2t} - B_3 V_{3t})$$

where  $\dot{W}$  is the rate of work done by the fluid and  $M$  is the moment/torque produced on the shaft by the fluid. Finally, application of the conservation of energy equation yields:

$$\dot{W} = \dot{m} \left[ \left( h_2 + \frac{1}{2} V_2^2 \right) - \left( h_3 + \frac{1}{2} V_3^2 \right) \right]$$

Once the geometry of the turbomachine is known, these equations can be used to characterise its performance at any instant. These equations are in general only valid for steady-state operation, but can also be applied in the quasi-static sense if it is recognised that the turbine rotational speed will change as a function of the net moment on the shaft:

$$\frac{\Delta\omega}{\Delta t} = \frac{M_{net}}{I}$$

where  $I$  is the rotational moment of inertia of the turbomachine around its axis of rotation. The net moment on the shaft is equal to the sum (taking direction into account) of the moments caused by the fluid, the generator (for the turbine), the motor (for the compressor) and friction.

### 5.3. Heat Exchangers

The solar receiver, recuperator and heat sink are three separate components (all can be classed as “heat exchangers”), but the methods used to analyse them are very similar. The solar receiver is of the parabolic trough/evacuated tube type, the recuperator is of the printed circuit type and the heat sink is simply a finned tube. The geometry of each of these components is essentially a single flow channel (or a series of identical parallel flow channels). Each channel can then be divided into several small, one-dimensional control volumes. The conservation equations are then applied to each control volume, and the solution at each time step of the simulation is calculated using an explicit finite difference scheme.

The form of the conservation equations given by [19] are well-suited to be applied to this approach. In particular, [19] presents a particular form of the conservation of energy equation which expresses the internal energy of the control volume as the subject.

Consider the conservation of momentum principle, as applied to a one-dimensional cylindrical control volume and in the absence of gravitational forces; depicted in Fig. 7.

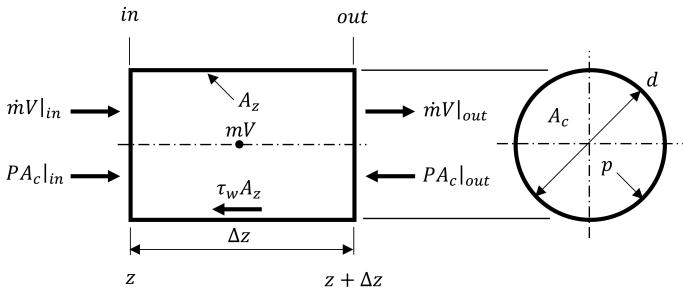


**Fig. 7. Conservation of momentum principle as applied to a one-dimensional cylindrical control volume**

Assuming that flow enters the control volume at the left boundary (at  $z$ ) and exits at the right boundary (at  $z + \Delta z$ ), the conservation of momentum of the control volume is, from [19]

$$\frac{\Delta(mV)}{\Delta t} = (\dot{m}V)_{in} - (\dot{m}V)_{out} + (PA_c)_{in} - (PA_c)_{out} - \tau_w A_z$$

which states that the time rate of change of momentum  $mV$  of a control volume is equal to, the sum of:

- the net rate of momentum  $\dot{m}V$  entering the control volume,
- the net external force  $PA_c$  applied on the control volume as a result of pressure on its cross-sectional surfaces, and
- the frictional force, expressed as a wall shear stress  $\tau_w$  acting on the walls of the element with area  $A_z$

As is the basis of the explicit solution method, all the terms on the right of the equation are to be evaluated at the current time step and are therefore all known values.

Note that the cross-sectional area is calculated as

$$A_c = \frac{\pi d^2}{4}$$

and the wall area is calculated as

$$A_z = \pi d \Delta z = p \Delta z$$

where  $d$  is the diameter of the control volume,  $p$  is the perimeter of the control volume and  $\Delta z$  is the length of the control volume.

Similarly, consider the conservation of energy principle, as applied to a one-dimensional cylindrical control volume and in the absence of gravitational forces; depicted in Fig. 8:

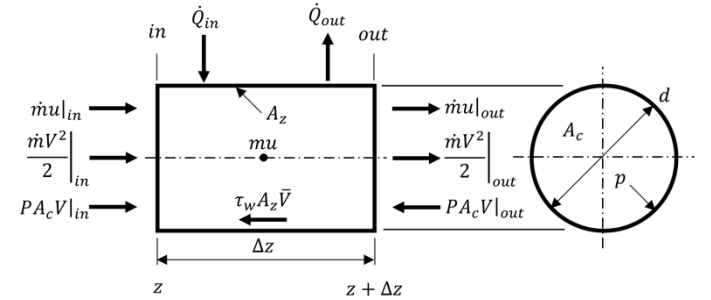


**Fig. 8. Conservation of energy principle as applied to a one-dimensional cylindrical control volume**

Assuming again that flow enters the control volume at the left boundary (at  $z$ ) and exits at the right boundary (at  $z + \Delta z$ ), and that heat can be conducted into or out of each control volume through its cylindrical wall; then the conservation of energy of the control volume is, from [19]

$$\frac{\Delta(mu)}{\Delta t} = (\dot{m}u)_{in} - (\dot{m}u)_{out} + \dot{Q}_{in} - \dot{Q}_{out} + (PA_c V)_{in} - (PA_c V)_{out} - \tau_w A_z \bar{V}$$

which states that the time rate of change of internal energy  $mu$  of a control volume is equal to, the sum of:

- the net rate of internal energy  $\dot{m}u$  entering the control volume by convective transport,
- the net rate of heat transfer  $\dot{Q}$  into the control volume by conduction (which is to say a heat transfer that arises as a result of the temperature difference between the control volume and its environment),
- the net rate of work done by the pressure forces  $PA_c V$  (which is *reversible*), and

- the heat generated in the fluid as a result of the friction work (viscous dissipation) in the fluid (which is *irreversible*) – calculated as the product of the shear force  $\tau_w A_z$  and the average velocity of the fluid  $\bar{V}$  in the control volume

The kinetic energy terms  $\dot{m}V^2/2$  curiously do not appear in this form of the conservation of energy equation, known as the *conservation of internal energy*. It is however just as valid as the more elaborate *conservation of total energy* form [19].

The preceding equations are all sufficient for numerical calculation purposes. But, it can be shown that in the limit as the control volume length tends to zero, these finite volume equations are identical to the partial differential conservation equations commonly reported in engineering literature.

The conservation of mass principle can be applied in a similar fashion and has the form

$$\frac{\Delta m}{\Delta t} = \dot{m}_{in} - \dot{m}_{out}$$

But, the assumption of quasi-static equilibrium stipulates that  $\dot{m}_{in} = \dot{m}_{out}$ , and hence that

$$\frac{\Delta m}{\Delta t} = 0$$

The implication of this is that the conservation of mass equation cannot be solved to determine the mass of a control at the next time step. Instead, after the mass flow rate for the next time step is determined using another method (for example, by considering the work input and upstream conditions of the compressor), the definition of the mass flow rate is used to find the density

$$\rho = \frac{\dot{m}}{VA_c}$$

and the definition of density (the ratio of mass  $m$  to volume  $v$ ) can then be used to find the mass

$$m = \rho v = \rho A_c \Delta z$$

The terms  $\dot{Q}_{in}$  and  $\dot{Q}_{out}$  represent the external heat transfer into or out of the control volumes. [21] presents a very detailed model for the solar thermal heat input ( $\dot{Q}_{in}$ ) to a parabolic trough receiver, which will be used in this project.  $\dot{Q}_{out}$  is determined from a complete heat transfer analysis, based on the known control volume temperatures at the current time step. Conduction, convection (natural and forced) and radiation are taken into account. Material properties are taken to vary as functions of temperature. The heat transfer rates out of the control volumes  $\dot{Q}_{out}$  are evaluated for both the solar receiver and the heat sink.

The recuperator is assumed to be well-insulated such that heat is transferred only through convection between the fluid streams and the wall separating the streams, and conduction through the wall itself.

## 6. Modelling Results

To showcase the capability of the modelling methodology some results are presented. Using the velocity triangle approach as described in §5.2 as basis, an illustrative turbine model as shown in Fig. 9 can be produced. Fig. 9a shows the overall efficiency  $\eta_o$  (the isentropic efficiency of the turbine corrected for windage, leakage and bearing friction) as a function of the turbine speed  $N$  and mass flow rate  $\dot{m}$ . Fig. 9b shows the overall efficiency of the turbine as a function of the speed and pressure ratio  $P_1/P_3$ . Similar plots for any combination of variables can be generated easily from the turbine model.

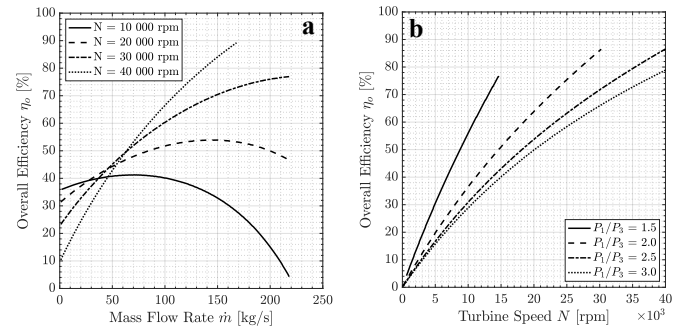


Fig. 9. Illustrative turbine model

Next, is an illustrative example of how the control volume approach of §5.3 can be used to model the counter-current recuperator heat exchanger. Using 30 control volumes per stream, the temperature in each control volume and pressure drop along the length of the heat exchanger is plotted in Fig 10. The hot stream is plotted as flowing from left-to-right, and the cold stream is plotted as flowing from right-to-left. Notice that, despite both streams flowing along the same length of heat exchanger and with the same cross-sectional flow channel area, the pressure drop in the hot stream is significantly higher than that of the cold stream: a consequence of the lower density and higher velocity of the hot stream.

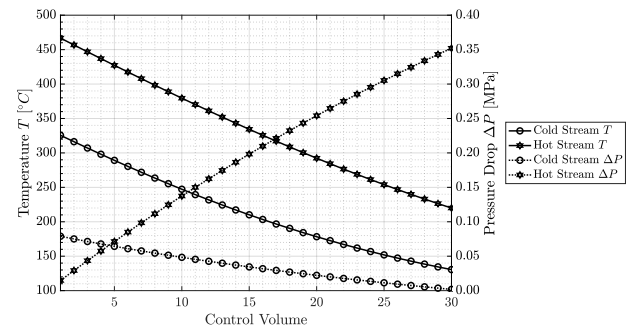


Fig. 10. Recuperator heat exchanger model

## 7. Simulation

After the individual models of the turbomachinery and heat exchangers have been developed, a unified system model can be created and the simulation campaign can commence. Some examples of the scenarios that can be simulated are:

- System start-up, operation and shut-down under design DNI and environmental conditions
- Variable DNI profile, representative of a typical sunny (no cloud cover) day, from sunrise to sunset
- Variable DNI profile, representative of a day with intermittent sunshine (e.g. partly cloudy)
- DNI profiles representative of different seasonal cases
- Operation under different ambient conditions (air temperature or wind speed)

## 8. Conclusion

The benefits and challenges of using sCO<sub>2</sub> as working fluid in CSP plants were discussed. The reasons for developing a simulation of a CSP-sCO<sub>2</sub> plant were highlighted, and it was mentioned how this simulation is not only applicable to the CSP field, but also to further the study of sCO<sub>2</sub> cycles in general. Numerical studies by other authors for the purpose of validating the models and simulation of this work were given.

After introducing the CSP-sCO<sub>2</sub> cycle to be simulated, the simulation and modelling methodology were presented. Illustrative models of the turbomachinery and recuperator heat exchanger were showcased and an overview of the simulation campaign was given.

## Acknowledgements

The authors would like to thank the Centre for Renewable and Sustainable Energy Studies (CRSES) at Stellenbosch University for funding.

## References

1. U.S Department of Energy. 2015. *Quadrennial Technology Review 2015: Supercritical Carbon Dioxide Brayton Cycle*. Technical report.
2. Stein, W. & Buck, R. 2017. Advanced power cycles for concentrated solar power. *Solar Energy*.
3. Santini, L., Accornero, C. & Cioncolini, A. 2016. On the adoption of carbon dioxide thermodynamic cycles for nuclear power conversion: A case study applied to Mochovce 3 Nuclear Power Plant. *Applied Energy*, 181:446–463.
4. Sandia National Laboratories. 2011. *Supercritical carbon dioxide Brayton Cycle turbines promise giant leap in thermal-to-electric conversion efficiency*. Sandia Labs News Release, March 4.
5. Dostal, V., Driscoll, M. & Hejzlar, P. 2004. *A Supercritical Carbon Dioxide Cycle for Next Generation Nuclear Reactors*. Technical Report MIT-ANP-TR-100, MIT.
6. Milani, D., Luu, M.T., McNaughton, R. & Abbas, A. 2017. Optimizing an advanced hybrid of solar- assisted supercritical CO<sub>2</sub> Brayton cycle: A vital transition for low-carbon power generation industry. *Energy Conversion and Management*, 148:1317–1331.
7. Cheang, V., Hedderwick, R. & McGregor, C. 2015. Benchmarking supercritical carbon dioxide cycles against steam Rankine cycles for Concentrated Solar Power. *Solar Energy*, 113:199–211.
8. Avadhanula, V.K. & Held, T.J. 2017. Transient modeling of a supercritical CO<sub>2</sub> power cycle and comparison with test data. *Proceedings of ASME Turbo Expo 2017: Turbomachinery Technical Conference and Exposition*, GT2017-63279.
9. Kim, M.S., Oh, B.S., Kwon, J.S., Jung, H-Y. & Lee, J.I. 2017. Transient simulation of critical flow with thermal-hydraulic system analysis code for supercritical CO<sub>2</sub> applications. *Proceedings of ASME Turbo Expo 2017: Turbomachinery Technical Conference and Exposition*, GT2017-63549.
10. Dyreby, J.J. 2014. Modeling the Supercritical Carbon Dioxide Brayton Cycle with Recompression. Doctoral dissertation: University of Wisconsin-Madison.
11. Neises, T. & Turchi, C. 2014. A comparison of supercritical carbon dioxide power cycle configurations with an emphasis on CSP applications. *Energy Procedia*, 49:1187-1196.
12. Osorio, J.D., Hovsopian, R. & Ordonez, J.C. 2016. Effect of multi-tank thermal energy storage, recuperator effectiveness, and solar receiver conductance on the performance of a concentrated solar supercritical CO<sub>2</sub>-based power plant operating under different seasonal conditions. *Energy*, 115: 353-368.
13. Couso, G.B., Vicencio, R.B., Padilla, R.V., Soo Too, Y.C. & Pye, J. 2017. Dynamic model of supercritical CO<sub>2</sub> Brayton cycles driven by concentrated solar power. *Proceedings of the ASME 2017 11th International Conference on Energy Sustainability*, ES2017-3573.
14. Ortega, J., Khivsara, S., Christian, J., Ho, C., Yellowhair, J. & Dutta, P. 2016. Coupled modeling of a directly heated tubular solar receiver for supercritical carbon dioxide Brayton cycle: Optical and thermal-fluid evaluation. *Applied Thermal Engineering*, 109:970-978.
15. Conboy, T.M., Carlson, M.D. & Rochau, G.E. 2014. Dry-cooled supercritical CO<sub>2</sub> power for advanced nuclear reactors. Presentation at the ASME Turbo Expo 2014, June 16-20, Dusseldorf, Germany
16. Friedman, P. & Anderson, M. 2017. Thermodynamics, in Brun, K., Friedman, P. & Dennis, R. (editors). *Fundamentals and Applications of Supercritical Carbon Dioxide (sCO<sub>2</sub>) Based Power Cycles*. Duxford: Woodhead Publishing.
17. Sienicki, J.J., Moisseytsev, A., Fuller, R.L., Wright, S.A. & Pickard, P.S. 2011. Scale Dependencies of Supercritical Carbon Dioxide Brayton Cycle Technologies and the Optimal Size for a Next-Step Supercritical CO<sub>2</sub> Cycle Demonstration. SCO<sub>2</sub> Power Cycle Symposium, May 24-25, Boulder, Colorado.
18. White, F.M. 2011. *Fluid Mechanics*. London: McGraw-Hill Education.
19. Bird, R.B., Stewart, W.E. & Lightfoot, E.N. 2002. *Transport Phenomena*. New York: John Wiley & Sons, Inc.
20. Dixon, S.L. & Hall, C.A. 2014. *Fluid Mechanics and Thermodynamics of Turbomachinery*. Oxford: Butterworth-Heinemann.
21. Patnode, A.M. 2006. Simulation and Performance Evaluation of Parabolic Trough Solar Power Plants. Master's thesis: University of Wisconsin-Madison.